

Structured metal thin film as an asymmetric color filter: The forward and reverse plasmonic halos

Authors: F. Ye, Michael J. Burns, Michael Naughton

Persistent link: <http://hdl.handle.net/2345/bc-ir:107161>

This work is posted on [eScholarship@BC](#),
Boston College University Libraries.

Published in *Scientific Reports*, vol. 4, 2014

This work is licensed under a Creative Commons Attribution-NonCommercial-NoDerivs 4.0 International License (<http://creativecommons.org/licenses/by-nc-nd/4.0/>).



OPEN

SUBJECT AREAS:

NANOCAVITIES

MICRO-OPTICS

OPTICAL SENSORS

IMAGING AND SENSING

Structured metal thin film as an asymmetric color filter: the forward and reverse plasmonic halos

Fan Ye, Michael J. Burns & Michael J. Naughton

Department of Physics, Boston College, Chestnut Hill, MA, 02467, USA.

Received
3 July 2014Accepted
14 November 2014Published
1 December 2014Correspondence and
requests for materials
should be addressed to
M.J.N. (naughton@bc.
edu)

We observe asymmetric color filtering under unpolarized incidence in a structured metallic (Ag) film, where the center of an optically thick circular Ag disk surrounded by a step gap appears dark when observed from one side, and bright from the other. The latter situation corresponds to abnormally high optical transmission through the optically thick film. We explain this by a three-step process: coupling of photons to surface plasmon polaritons (SPPs), wave interference of SPPs forming resonant cavity modes, and out-coupling from SPPs to photons. Full wave electromagnetic simulations based on the finite element method support our findings. These results may have potential applications in areas such as optical color filtering and biosensing via dielectric detection within the step gap plasmonic cavity.

Surface plasmon polaritons (SPPs) are two dimensional electron density waves that can propagate along and are confined to a metal-dielectric interface. First proposed by Langmuir *et al.* in 1929, plasmons are collective excitations of electrons in a metal¹. That plasmons can be excited along a metal-dielectric interface and then propagate as SPPs was noted by Ritchie in 1957². SPPs have gained significant attention in recent years, perhaps especially since a report of extraordinary optical transmission through sub-wavelength hole arrays on metal films by Ebbesen *et al.*^{3,4}. Due to the advancement of fabrication and calibration techniques, research on novel applications based on SPPs and their cavity modes is expanding, recent examples of which include plasmonic waveguiding^{5,6}, focusing^{7,8}, and color filtering^{9–11}.

Most recently, researchers are exploring the possibilities of achieving asymmetric propagation of electromagnetic (EM) waves via 2D (or quasi-2D) symmetry-broken structures^{12,13}. These works break the symmetry between forward and backward travelling EM waves by generating asymmetric plasmon modes locally in the asymmetric metallic structures. Although not in the real sense an optical isolator¹⁴, these effects can have a wide range of optoelectronic applications^{12,13}. We show here a new version of symmetry-broken EM propagation, realized by breaking the geometrical symmetry on different sides of a nanostructured device. Our design has axial symmetry, and thus has minimum requirements on the polarization state of incident light, such that it works for even unpolarized incidence.

In previous work, we demonstrated SPP drumhead modes within circular structures¹¹. An example of an SPP drumhead cavity surrounded by a circular step gap is shown in Fig. 1 (adapted from Ref. 11). When light is injected from the bottom side of this device, one observes transmitted light leaking into the far field around the step gap circumference. As reported in Ref. 11, the spectrum of this leaked light is modulated by the formation of resonant SPP standing waves (drumhead modes) on the circular cavity surface, yielding a “plasmonic halo” effect¹¹. Here, we present another phenomenon related to this step gap drumhead structure, found by simply reversing the direction of illumination. That is, when light is injected from the top side, one observes that the center of the SPP drumheads always appears bright, in strong contrast to the “plasmonic halo” case, where one sees a dark center of the drumheads. This is anomalous because in the central region, where strong far-field light intensity is observed, the Ag film is optically thick (300 nm), forbidding any direct transmission of photons. In other words, via the step-gap circular drumhead structure, it appears as though photons transmit through an optically thick metal film. We call this a “reverse halo” effect due to its close relation to the plasmonic halo effect, but with the light direction reversed. As we show below, the physical origin of this counterintuitive reverse halo phenomenon lies in a three-step coupling process: incident photons are coupled into SPPs, which then propagate and interfere along the metal/dielectric interface, forming standing waves, which couple back into photons via multiple scattering mechanisms. The reverse halo effect, together with the plasmonic halo, make the structured Ag film work somewhat like an optical rectifier might, with the center of the Ag disk being bright when

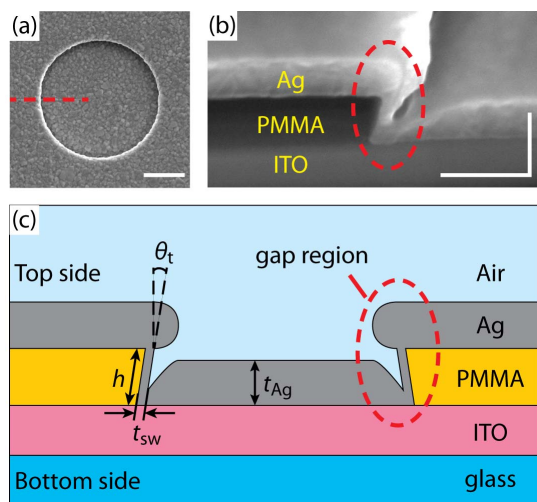


Figure 1 | Sample structure. (a) Top view of the SEM micrograph of a circular Ag step-gap cavity. (b) 45-degree tilted view of the cross-section of a circular Ag step-gap cavity, with cross-section position indicated by red dotted line in (a). (c) Schematic cross-section of a circular Ag step-gap cavity, with parameters defined, top and bottom sides defined, and gap region indicated by a red dotted circle. Scale bar in (a), 1 μm ; horizontal and vertical scale bars in (b), 500 nm.

illuminated from one side, and dark when illuminated from the other side. The device, however, is not an optical rectifier or diode in the real sense, since it does not break time-reversal symmetry of an electromagnetic wave¹⁴. Nonetheless, its asymmetric transmission property can have practical applications, such as asymmetric optical color filtering and biosensing via dielectric detection.

Results

Fig. 1 shows SEM micrographs and design details of the circular step-gap SPP cavity. Fig. 1(a) shows an SEM micrograph of the top view of one cavity with 2.85 μm diameter. Fig. 1(b) shows a 45-degree tilted view SEM micrograph of a cross-section taken along the line indicated in Fig. 1(a). The cross-section was cut by focused ion beam milling. Fig. 1(c) shows a schematic design of the step gap structure. The fabrication process was as follows: a layer of PMMA 495 (poly methyl methacrylate, a type of resist for electron beam lithography (EBL)) was spin coated on to an indium tin oxide (ITO, 500 nm) coated glass slide; circular patterns were defined on the PMMA layer via EBL and a layer of Ag was sputtered onto the patterned PMMA layer. Due to the quasi-directional nature of the sputtering process, when the deposited Ag is optically thick ($t_{\text{Ag}} \sim 300$ nm), its side wall thickness in the step gap remains optically thin ($t_{\text{sw}} \sim 50$ nm), allowing direct tunneling of SPPs and photons.

Fig. 2 shows optical images of light transmitted past arrays of the circular step-gap cavities, with radii of 3.0, 2.0 and 1.2 μm , top to bottom, under different illumination schemes. All images were taken in a Leica DM6000M optical microscope, with a 50 \times objective (NA = 0.8). Fig. 2(a) shows the transmission optical images when unpolarized white light (from a halogen lamp) is injected from the bottom side of the samples, as observed from the top side. Fig. 2(b) shows transmission images for the same samples as (a), but with the light injected from the top side, and observed from the bottom. The feature that Figs. 2(a) & (b) have in common is the bright ring at the step-gap circumference of each circular cavity. The prominent difference between the image sets is that the centers of the cavities are dark in Fig. 2(a), while being bright in Fig. 2(b). Fig. 2(c) & 2(d) show expanded views of a selected structure, with the field intensity across the center (indicated by dashed red lines) plotted on the right hand

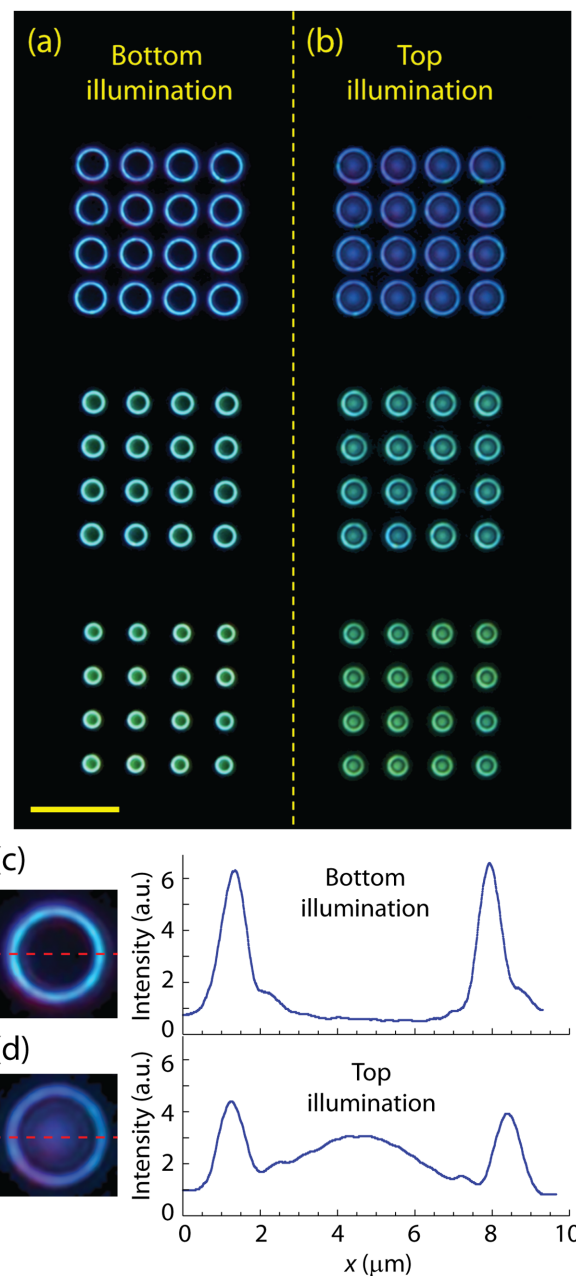


Figure 2 | Optical images. (a) Transmission optical micrographs of the top side of arrays of circular step-gap cavities with various radii under unpolarized white light illumination from the bottom. (b) Transmission optical micrographs of the bottom side of the same devices as shown in (a) under the same light illuminated from the top. (c) & (d), Zoom in of one structure, with intensity plotted across center of structure (indicated by dashed lines) shown on the right, for bottom and top illumination configurations. Scale bar in (a) & (b): 20 μm .

side, showing an over 5 fold contrast of electric field intensity in the center of the structure.

Discussion

Two dimensional full wave electromagnetic simulations (using COMSOL MultiPhysics 4.3b) with axial symmetry were carried out to assist in our understanding of this phenomenon. As shown in Fig. 3, a plane wave is incident from the top side of the structure, with a k vector along the $-z$ direction, H vector pointing out of plane, and E vector pointing in the horizontal, radial direction. When revolved 360 degrees, this corresponds to the situation of radially

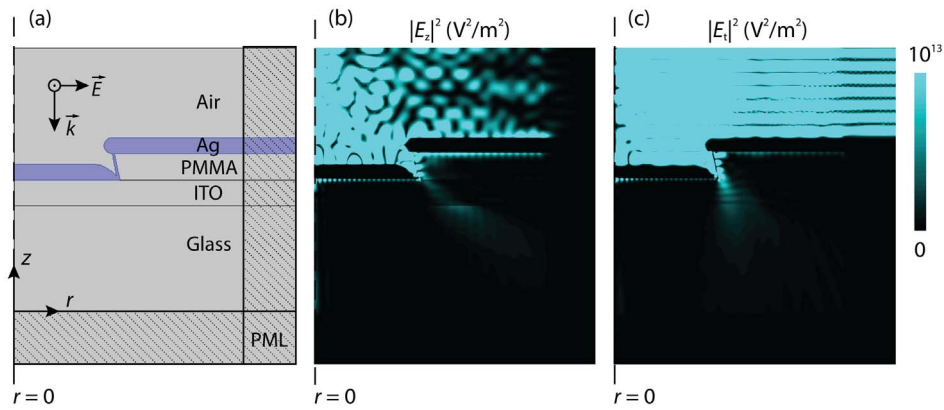


Figure 3 | Two dimensional full wave simulation with axial symmetry. (a) Schematic of simulated structure, with axis of symmetry labeled ($r = 0$). Perfectly matched layers (PML) on the right and bottom sides are indicated by hatched regions. Light is input from the top side. (b) & (c) Profiles of intensities of the vertical component $|E_z|^2$ (b) and transverse component $|E_t|^2$ (c) of the electric field for 490 nm incidence, under the same color scale ranging from 0 to 10^{13} V²/m².

polarized electric field input. Although this excitation scheme is not identical to that employed in the experiments, it mimics the unpolarized nature of the incident light. The simulated circular cavity has a diameter of 4 μm , with other parameters defined in Fig. 1(c). The transverse electric field is obtained by $|E_t|^2 = |E_r|^2 + |E_\theta|^2$. The incident electric fields are first coupled to SPPs and travel to the bottom side of the Ag/ITO interface through the step gap region, as shown in Fig. 3(b). The SPPs then form resonant drumhead modes along the circular Ag/ITO interface, resulting in a center intensity maximum. This SPP focusing phenomenon along circular geometries is widely observed and studied^{7,11,15}. The down-propagating electric field has two origins: one is from direct tunneling through the optically thin step gap region, resulting in the bright outer rings similar to those seen in the plasmonic halo effect; the other is from coupling from the SPP component in the form of radiation loss of SPPs due to surface and grain-boundary scattering on the Ag/ITO interface¹⁶, resulting in the bright centers of the step gap cavities. The reasons for a much weaker radiation coupling effect on the Ag/air interface when illuminating from the bottom (the plasmonic halo) than on the Ag/ITO interface (the reverse halo) are twofold. First, the Ag/ITO interface on the bottom has an open optical boundary below it. With no other forms of modes to couple to, the SPPs along the Ag/ITO interface are scattered directly into free propagating photons, as opposed to the Ag/air interface on top, which is within a circular cavity formed by the step-gap, allowing the SPP-generated photons to interfere with photons directly tunneled through the step-gap¹¹. Second, for SPPs, the Ag/ITO interface has a much larger effective radius than the Ag/air interface with the same physical dimension. For example, for incident light with 490 nm free space wavelength, the SPP wavelength along a Ag/air interface ($\lambda_{\text{SPP}}^{\text{(air)}} = 459$ nm) is ~ 5 times that along a Ag/ITO interface ($\lambda_{\text{SPP}}^{\text{(ITO)}} = 87$ nm), indicating a corresponding increase in the effective radius along the Ag/ITO interface. This much larger effective radius along the Ag/ITO interface assists the SPP-photon coupling process¹⁶. Furthermore, the higher dielectric constant of ITO effectively increases the surface roughness and grain boundary size of the Ag film along the Ag/ITO interface, enlarging the radiation loss of SPPs. In summary, the geometric difference and the dielectric environment difference result in a drastically different out-coupling pathway for bound SPPs, leading to the bright/dark contrast of the top and bottom Ag surface under two illumination schemes.

The above argument alone, however, does not fully explain the observed phenomenon. The SPP standing wave-induced far-field component should have nodes and anti-nodes, like the SPP drumhead mode patterns along the circular Ag/ITO interface simulated in Fig. 4(b). The experimentally observed center bright spot, however, is

blurred out, as shown in more detail in Fig. 4(d). This can be explained by the Abbe diffraction limit $\lambda/(2\text{NA})$ of an optical microscope¹⁷. The sample images were taken with a 50 \times objective lens, with NA = 0.8. Thus, the resolution limit is $\sim \lambda/1.6$ for the obtained reverse halo images. For a 490 nm incident light, this limit is calculated to be 306 nm, 3.5 times larger than the calculated periodicity of the nodes and antinodes of SPP standing waves along the Ag/ITO interface, which is about $\lambda_{\text{SPP}}^{\text{(ITO)}} = 87$ nm under 490 nm light. Fig. 4(c) shows the same field profile as Fig. 4(b), after numerically signal averaging over an area with 306 nm diameter to mimic the resolution limit in our optical microscope. The color scales in Fig. 4(a), (b) & (c) are chosen so as to match the experimental data shown in Fig. 4(d). After this averaging associated with the diffraction limit, the smoothed center bright spot agrees well with the measured result. This is the main result of this paper. In principle, sub-diffraction-limit microscopy, such as NSOM, could resolve the blurred standing wave patterns. This is not possible with the present sample configuration, however, due to the thickness of the glass substrate on the bottom side.

To put the above results in context, we show in Fig. 5 a simulation for the bottom illumination situation under the same incidence condition for the same structure as Fig. 4, generating the plasmonic halo effect¹¹. Figure 5(a) shows the profile of transverse (in-plane) electric field intensity at the cross-section of a circular step gap structure, where the dark center within the circular step gap cavity is clearly presented. If we take a cross-section within the circular cavity, we will see a dark center surrounded by a circular bright ring, as shown in Fig. 5(b). Simulation results shown in Fig. 4(c) and 5(b) closely represent the measured data in Fig. 2 (c) and (d), confirming the SPP-related physical nature of this phenomenon.

Figure 6 shows the transmission spectrum of the same circular structure as in Fig. 4, under the same illumination condition with incident wavelength swept from 450 to 750 nm. The sharp transmission peak at around 490 nm corresponds to the bright center mode shown in Fig. 4. As analyzed in detail in Ref. 11, the side wall length of the step-gap structure, together with the radius of the circular cavity, determine the spectral response of the device over the visible range. The two transmission minima between 550 to 600 nm are caused by SPP drumhead modes within the circular step gap¹¹.

Unlike optical isolators, which require breaking of time-reversal symmetry to create nonreciprocity^{18–20}, asymmetric light propagation in reciprocal systems works by breaking chiral symmetry (handedness)^{21–24} or geometry^{13,25,26}. While some designs generate asymmetric transmission for circularly polarized incidence^{21–24}, others show asymmetric propagation for linearly polarized light^{25–28}. One of the advantages of our circular step gap structure is its intrinsic

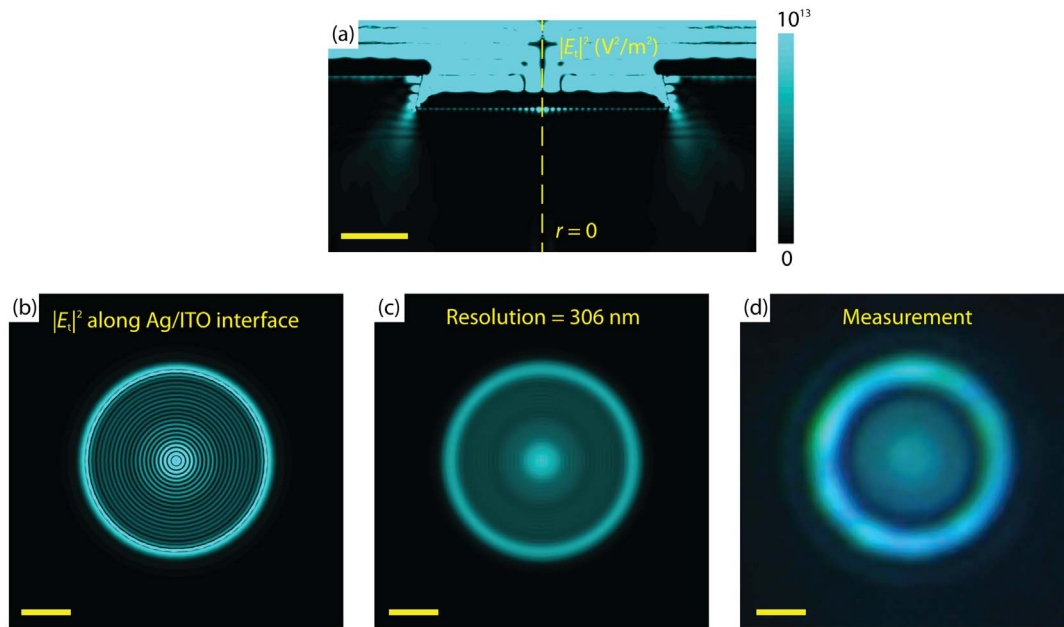


Figure 4 | Physical origin of the “reverse halo” effect. (a) Cross-section view of the simulated in-plane electric field intensity $|E_t|^2$ for a circular cavity with 4 μm diameter under 490 nm unpolarized incidence from top. (b) Simulated in-plane electric field intensity $|E_t|^2$ distribution at the Ag/ITO interface for the same structure as (a) and under the same illumination condition. (c) Electric field intensity in (b) averaged over an area with 306 nm diameter, mimicking the resolution limit of an optical microscope. (d) Transmission optical micrograph of a circular SPP cavity under unpolarized white light illumination from the top side. Scale bars, 1 μm . Color scales in (a), (b) & (c) are the same, ranging from 0 to 10^{13} V^2/m^2 , as shown by the color scale on the right.

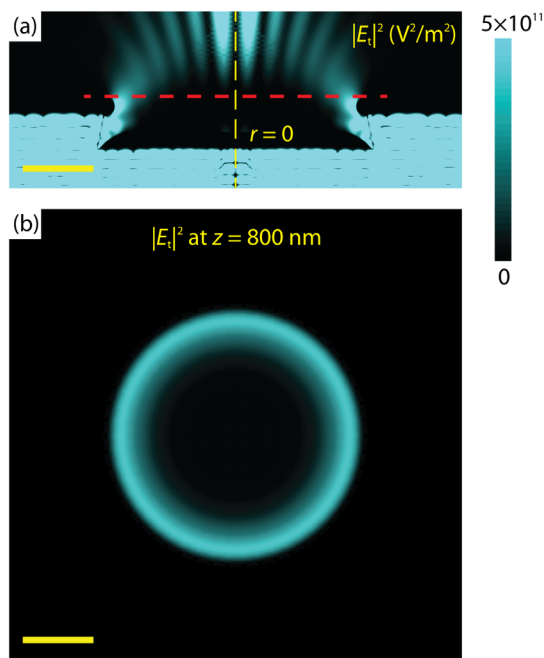


Figure 5 | Field distribution of the “plasmonic halo” effect. (a) Cross-section view of the simulated in-plane electric field intensity $|E_t|^2$ for a circular cavity with 4 μm diameter under 490 nm unpolarized incidence from bottom. (b) Simulated in-plane electric field intensity $|E_t|^2$ distribution at the top surface (as indicated by a red dashed line in (a)) for the same structure as (a) and under the same illumination condition. Scale bars, 1 μm . Color scales in (a) & (b) are the same, ranging from 0 to 5×10^{11} V^2/m^2 , as shown by the color scale on the right.

property of axial symmetry, making it compatible with both linearly and circularly polarized, and even unpolarized, light. In fact, the optical images in Fig. 2 are taken under unpolarized illumination.

In conclusion, we have shown a novel optical phenomenon that works as an asymmetric color filter, where the center of an optically thick circular Ag disk surrounded by step gap appears dark when observed from one side, and bright from the opposite side. The step-gap structure, together with the different dielectric environments on both sides of the Ag film, breaks the geometrical symmetry on the device, yielding this asymmetric phenomenon. Through full wave electromagnetic simulations, we demonstrated the physical origin of this “reverse halo” effect as a three-step coupling process: photons couple into SPPs, which propagate and interfere along a circular metal surface, yielding a maximum intensity at its center, before

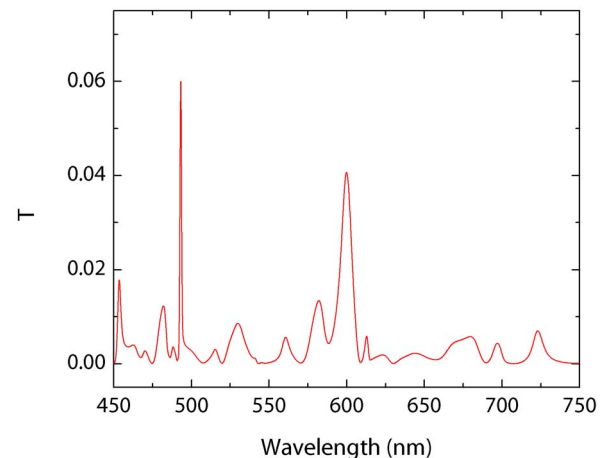


Figure 6 | Transmission (T) spectrum of the “reverse halo”. Transmission spectrum of the same circular step gap structure as in Fig. (4) under the same illumination condition, with incident wavelength swept from 450 nm to 750 nm.



finally coupling back into photons through radiation loss. This asymmetric color filter based on forward and reverse plasmonic halos can have potential applications in areas such as optical color filtering and biosensing via dielectric detection within the step gap SPP cavity.

Methods

Device fabrication and characterization. The fabrication process for the step-gap plasmonic circular cavities is as follows. A poly(methyl methacrylate 495) (PMMA) layer was first spin coated onto an indium tin oxide- (ITO) coated glass substrate, then baked on a hot plate for 90 sec at 180°C. The thickness of the ITO layer was about 500 nm. The thickness of the PMMA coating was controlled by spin speed and solution concentration. ITO-coated glass substrates were chosen to enable stable electron beam writing, as well as high optical transmittance in the visible range. Electron beam lithography was done on the PMMA-coated substrates in the Boston College Integrated Sciences Clean Room facility, forming arrays of circular holes with radii ranging from 1.0 to 3.0 μm . The spacing between individual circular holes is chosen to be 10 μm . Development was done in an MIBK:IPA = 1:3 solution for 2 min. Samples were baked on a hot plate at 100°C for 1 min before being loaded into the sputtering chamber. 300 nm of Ag was sputtered onto the samples at a base pressure of 2×10^{-5} Pa in an AJA Int'l Inc. sputter system. Sputtering was done in DC mode, at a constant output power of 200 W. Silver thickness was controlled by deposition time after calibration with a quartz crystal monitor. Note that no lift-off process is needed. Transmission optical images are obtained by a 50 \times objective (NA = 0.8) in the Leica DM 6000 M Optical Microscope.

Numerical simulations. The mode profiles shown in Figs. 3 & 4 were obtained by finite element electromagnetic simulations in COMSOL Multiphysics 4.3b. Two dimensional simulations with axial symmetry were carried out, with plane wave incident from the top side of the geometry (Fig. 3(a)), and perfectly matched layers (PML) covering the bottom and right side. The symmetry axis ($r = 0$) coincides with the left boundary of the geometry. Incident electric field is polarized along the r -axis, and magnetic field is polarized along the θ -axis, corresponding to an axially polarized optical beam. The spatial average of the simulated electric field intensity (shown in Fig. 4(c)) was done in OriginLab 8.1.

1. Tonks, L. & Langmuir, I. Oscillations in ionized gases. *Phys. Rev.* **33**, 195–210 (1929).
2. Ritchie, R. H. Plasma losses by fast electrons in thin films. *Phys. Rev.* **106**, 874–881 (1957).
3. Ebbesen, T. W., Lezec, H. J., Ghaemi, H. F., Thio, T. & Wolff, P. A. Extraordinary optical transmission through sub-wavelength hole arrays. *Nature* **391**, 667–669 (1998).
4. Barnes, W. L., Dereux, A. & Ebbesen, T. W. Surface plasmon subwavelength optics. *Nature* **424**, 824–830 (2003).
5. Oulton, R. F. *et al.* A hybrid plasmonic waveguide for subwavelength confinement and long-range propagation. *Nature Photon.* **2**, 496–500 (2008).
6. Fang, Z. *et al.* Plasmonic coupling of bow tie antennas with Ag nanowire. *Nano Lett.* **11**, 1676–1680 (2011).
7. Liu, Z. *et al.* Focusing surface plasmons with a plasmonic lens. *Nano Lett.* **5**, 1726–1729 (2005).
8. Fang, Z. *et al.* Plasmonic focusing in symmetry broken nanocorrals. *Nano Lett.* **11**, 893–897 (2011).
9. Laux, E., Genet, C., Skauil, T. & Ebbesen, T. W. Plasmonic photon sorters for spectral and polarimetric imaging. *Nature Photon.* **2**, 161–164 (2008).
10. Xu, T., Wu, Y.-K., Luo, X. & Guo, L. J. Plasmonic nanoresonators for high-resolution colour filtering and spectral imaging. *Nature Commun.* **1**, 59 (2010).
11. Ye, F., Burns, M. J. & Naughton, M. J. Plasmonic halos – optical surface plasmon drumhead modes. *Nano Lett.* **13**, 519–523 (2013).
12. Fedotov, V. A. *et al.* Asymmetric propagation of electromagnetic waves through a planar chiral structure. *Phys. Rev. Lett.* **97**, 167401 (2006).

13. Menzel, C. *et al.* Asymmetric transmission of linearly polarized light at optical metamaterials. *Phys. Rev. Lett.* **104**, 253902 (2010).
14. Jalas, D. *et al.* What is – and what is not – an optical isolator. *Nature Photon.* **7**, 579–582 (2013).
15. Ye, F., Merlo, J. M., Burns, M. J. & Naughton, M. J. Optical and electrical mappings of surface plasmon cavity modes. *Nanophotonics* **3**, 33–49 (2014).
16. Kuttge, M. *et al.* Loss mechanisms of surface plasmon polaritons on gold probed by cathodoluminescence imaging spectroscopy. *Appl. Phys. Lett.* **93**, 113110 (2008).
17. Abbe, E. Beiträge zur Theorie des Mikroskops und der mikroskopischen Wahrnehmung. *Arch. Mikrosk. Anat.* **9**, 413–468 (1873).
18. Yu, Z. & Fan, S. Complete optical isolation created by indirect interband photonic transitions. *Nature Photon.* **3**, 91–94 (2009).
19. Manipatruni, S., Robinson, J. T. & Lipson, M. Optical nonreciprocity in optomechanical structures. *Phys. Rev. Lett.* **102**, 213903 (2009).
20. Lira, H., Yu, Z., Fan, S. & Lipson, M. Electrically driven nonreciprocity induced by interband photonic transition on a silicon chip. *Phys. Rev. Lett.* **109**, 033901 (2012).
21. Fedotov, V. A. *et al.* Asymmetric transmission of light and enantiomerically sensitive plasmon resonance in planar chiral nanostructures. *Nano Lett.* **7**, 1996–1999 (2007).
22. Schwanecke, A. S. *et al.* Nanostructured metal film with asymmetric optical transmission. *Nano Lett.* **8**, 2940–2943 (2008).
23. Singh, R. *et al.* Terahertz metamaterial with asymmetric transmission. *Phys. Rev. B* **80**, 153104 (2009).
24. Plum, E., Fedotov, V. A. & Zheludev, N. I. Asymmetric transmission: a generic property of two-dimensional periodic patterns. *J. Opt.* **13**, 024006 (2011).
25. Wang, C., Zhong, X.-L. & Li, Z.-Y. Linear and passive silicon optical isolator. *Sci. Rep.* **2**, 674 (2012).
26. Ye, F., Burns, M. J. & Naughton, M. J. Symmetry-broken metamaterial absorbers as reflectionless directional couplers for surface plasmon polaritons in the visible range. *Adv. Opt. Mater.* **2**, 957–965 (2014).
27. Kang, M., Chen, J., Cui, H.-X., Li, Y. & Wang, H.-T. Asymmetric transmission for linearly polarized electromagnetic radiation. *Opt. Express* **19**, 8347–8356 (2011).
28. Feng, L. *et al.* Nonreciprocal light propagation in a silicon photonic circuit. *Science* **333**, 729–733 (2011).

Acknowledgments

This work was supported in part by the W. M. Keck Foundation.

Author contributions

This concept was proposed by M.J.B., with discussions with F.Y. and M.J.N. F.Y. designed the experiment, fabricated the samples and carried out numerical simulations. F.Y., M.J.B. and M.J.N. analyzed the data and wrote the manuscript.

Additional information

Competing financial interests: The authors declare no competing financial interests.

How to cite this article: Ye, F., Burns, M.J. & Naughton, M.J. Structured metal thin film as an asymmetric color filter: the forward and reverse plasmonic halos. *Sci. Rep.* **4**, 7267; DOI:10.1038/srep07267 (2014).



This work is licensed under a Creative Commons Attribution-NonCommercial-NoDerivs 4.0 International License. The images or other third party material in this article are included in the article's Creative Commons license, unless indicated otherwise in the credit line; if the material is not included under the Creative Commons license, users will need to obtain permission from the license holder in order to reproduce the material. To view a copy of this license, visit <http://creativecommons.org/licenses/by-nc-nd/4.0/>